Journal of Zhejiang University-SCIENCE B in press
www.jzus.zju.edu.cn; www.springer.com/journal/11585
E-mail: jzus_b@zju.edu.cn

Research Article

https://doi.org/10.1631/jzus.B2600138

Photobiomodulation with red light promotes drug-free vascular repair after balloon angioplasty

Shujie JIN[1], Xingwang WANG[1], Yijing YIN[1], Chengqiang YE[1], Peihong JI[2], Ya PENG[3], Kefeng REN[1,4]✉, Youxiang WANG[1]✉, Jian JI[1,5]

[1.] *MOE Key Laboratory of Macromolecular Synthesis and Functionalization, Department of Polymer Science and Engineering, Shaoxing Institute, Zhejiang University, Hangzhou 310058, China*
[2.] *Hangzhou Matrix Medical Technology Co. Ltd, Hangzhou 311100, China*
[3.] *Neurosurgery Department of the Third Affiliated Hospital of Soochow University, Changzhou 213003, China*
[4.] *Key Laboratory of Cardiovascular Intervention and Regenerative Medicine of Zhejiang Province, Department of Cardiology, Sir Run Run Shaw Hospital, Zhejiang University, Hangzhou 310016, China*
[5.] *State Key Laboratory of Transvascular Implantation Devices, the Second Affiliated Hospital Zhejiang University School of Medicine, Hangzhou 310009, China*

Abstract: Balloon angioplasty, though effective for vascular stenosis, inevitably induces vascular injury during dilation. The absence of clinical interventions to promote endothelial regeneration post-injury predisposes patients to late-phase complications including thrombosis, inflammation, and restenosis. Photobiomodulation (PBM) is a biological intervention that can have a regulatory effect. Red light as its primary wavelength shows significant therapeutic promise in cardiovascular and neuropsychiatric disorders, which is especially important in cases where medication cannot be used. In this study, we evaluated the effects of 640-nm PBM at various doses on endothelial cells (ECs) and vascular smooth muscle cells (SMCs). In vivo, balloon-injured rat abdominal aortas underwent transvascular red light irradiation (20 mW/cm², 3 min) via optical fibers. PBM promoted EC migration, proliferation, nitric oxide release, and CD31 expression while concurrently suppressing SMC proliferation and contractility. Rat model outcomes also confirmed PBM attenuated the vascular inflammation reaction and reduced neointimal hyperplasia. These findings show that PBM could be a viable strategy to enhance intima repair and mitigate balloon-associated vascular injury and restenosis.

Key words: Photobiomodulation; Endothelial cells; Vascular stenosis; Balloon injury; Intima repair

1 Introduction

Cardiovascular diseases (CVDs) are the predominant cause of death around the world (Tsao et al., 2023). Clinically, balloon angioplasty has emerged as a widely adopted and effective method for blood vessel dilation in treating vascular stenosis. However, vascular injury, an almost inevitable consequence of balloon angioplasty, often leads to the denudation of endothelial cells (ECs) at barotrauma sites (McEver, 2015). This denudation can

✉Kefeng REN, renkf@zju.edu.cn
Youxiang WANG, yx_wang@zju.edu.cn
Kefeng REN, https://orcid.org/0000-0001-5456-984X
Youxiang WANG, https://orcid.org/0000-0002-7821-9470

Received Mar. 1, 2026; Revision accepted June 21, 2026;
Crosschecked xxx. xx, 20xx

subsequently trigger platelet activation and adhesion, as well as leukocyte infiltration (Frodermann and Nahrendorf, 2018). Furthermore, the release of cytokines by inflammatory cells further stimulates smooth muscle cells (SMCs) switching to a proliferative phenotype, enhancing SMC proliferation and migration (Inoue et al., 2011; Qian et al., 2023). Post-angioplasty restenosis, driven by mechanical injury-induced inflammation, SMC proliferation and neointimal formation, remains a clinical challenge (Gaudino et al., 2017; Wu et al., 2024).

While current antiproliferative therapies (drug-coated balloons, drug-eluting stents) effectively reduce restenosis (Zhu et al., 2021), these drugs also delay the healing of endothelial injuries (Liu et al., 2021). There are also some situations where anti-proliferative drugs are not suitable for use, for example, in blood vessels in the brain. Thus, a therapeutic approach that selectively promotes endothelial repair while suppressing SMC proliferation would address a critical unmet need, yet no clinically established strategy currently achieves this balance. We hypothesize that a paradigm shift, from inhibiting pathological SMC proliferation to actively promoting physiological endothelial regeneration, may offer a more balanced and durable strategy for post-angioplasty vascular repair.

In 1967, Endre Mester, widely regarded as the pioneer of photobiomodulation (PBM), first reported that low-intensity light stimulates biological processes without causing thermal damage. PBM is a treatment method that stimulates cell activity and enhances the function of biological tissues by using specific wavelengths of light, such as red light (600-700 nm) and near-infrared light (780-1200 nm) with a power density ranging from 5 mW/cm² to 5 W/cm² (Selestin et al., 2024). In addition to improving neural regeneration (Lee et al., 2021; Ma et al., 2024), reducing inflammatory responses (Vasconcelos et al., 2015) and enhancing bone repair (Lu et al., 2024), promoting wound healing and angiogenesis are also important application areas of PBM (Stepanov et al., 2022). PBM treatment activates cytochrome C oxidase (Cox) which serves as a photoreceptor and a transducer of photo signals (Srinivasan and Avadhani, 2012). Photon absorption excites Cox, speeding electron transfer and ATP synthesis (Passarella et al., 1984; Greco et al., 1991; Yu et al., 1997). Nitric oxide (NO) inhibits Cox by competing with O_2 but PBM can dissociate NO from binding sites, restoring respiration (Karu et al., 2005). Nitric oxide synthase (NOS) contains flavin chromophores (FAD, FMN) and heme which are excitable in the red/NIR range, and photoactivation of NOS may also release NO (Pope and Denton, 2023; Balbi et al., 2025). Additionally, PBM regulates the cellular redox state, further impacting cellular gene expression and signaling pathways (; Chen et al., 2011; Farivar et al., 2014). Numerous reports indicate that noncytotoxic doses of red light PBM stimulate cell proliferation, contributing to tissue repair and reduction of inflammation (Vasconcelos et al., 2015; Stepanov et al., 2022).

Given the histological and pathophysiological similarities between the process of restenosis and wound healing in other living tissues, it is plausible to treat vascular injury and enhance endothelial growth after balloon angioplasty with an appropriate dose of red light irradiation. Scheerder et al. (2001) reported a decreased restenosis rate in coronary heart disease patients who received red laser PBM treatment. The results demonstrated a positive effect in the cardiovascular field. However, their research focused mainly on phenomenological conclusions and lacked exploration of underlying mechanisms. In this study, we used a 630-640 nm PBM system to investigate its dose-dependent effects on ECs and SMCs. We briefly explored the underlying cellular mechanisms to understand how PBM may promote vascular repair and regulate vasomotor tone. To validate a paradigm shift from suppression-based to regeneration-based vascular therapy, we used a balloon-induced injury rat model to observe the therapeutic effects (Fig. 1).

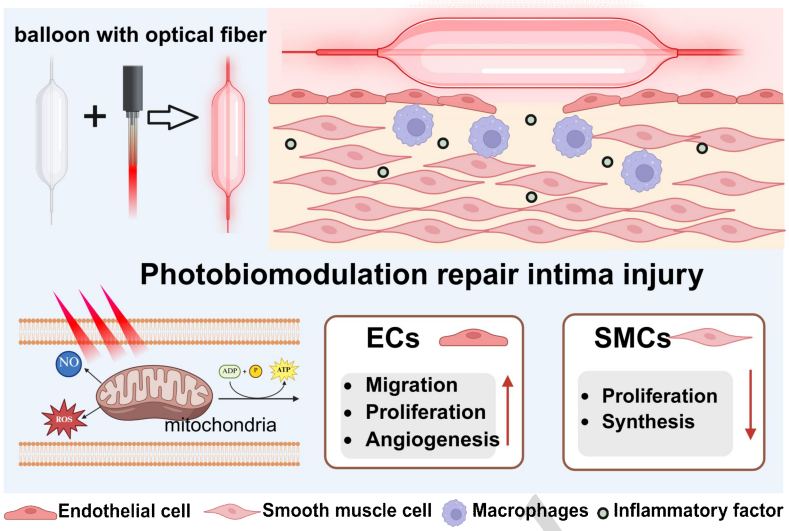

Fig. 1 Schematic diagram of PBM promoting intima repair.

2 Materials and methods

2.1 Cell culture

Human umbilical vein endothelial cells (HUVECs) and human arterial smooth muscle cells (HASMCs) used in our experiments were from 3 to 7 generations cultured at 37 ℃ in a humidified atmosphere containing 5% CO_2. EC culture medium, SMC culture medium and fetal bovine serum (FBS) were procured from ScienCell (USA). The culture medium was changed every 2 or 3 days to maintain optimal growth conditions.

2.2 Red light PBM treatment and power detection

The PBM light source was a 630-640 nm LED light purchased from Aijia electronic technology (Xuzhou, China). An Ophir Vega meter coupled with a 3A-P-FS-12 thermopile sensor (aperture Ø12 mm) was used to measure and calibrate the actual light power. LED light irradiated cells with an output power of 10 mW/cm², 20 mW/cm², or 30 mW/cm² for 3 min or 6 min, providing a light dose ranging from 1.8 to 10.8 J/cm².

2.3 Cell migration

Cells were seeded at a density of 100000 cells /well in 12-well cell culture plates. Once covered with cells, a 10-μL pipette tip was used to create a vertical scratch in the middle of each well. The cultures were washed with PBS to remove dead cells, ensuring a clear gap line was visible. Low serum DMEM medium (Gibco,USA) was used to minimize the influence of cell proliferation. Subsequently, cells were irradiated with red light, and the gap width was observed under a microscope (DS-Ri2, Nikon, Japan) at 0, 6, and 24 h post-irradiation to calculate the cell migration ratio.

2.4 Cell proliferation

Cells were seeded at a density of 5000 cells /cm² in 96-well cell culture plates and stained with CellTracker™ Green CMFDA Dye (Thermo, USA). Then the cell number at 0, 24, 48, and 72 h post PBM treatment was counted to observe the effect of PBM on cell proliferation. The cells during the synthesis phase were labeled by the incorporation of EdU using a BeyoClick™ EdU-488 Kit (Beyotime, China).

2.5 ATP assay

ATP production in cells was detected using CellTiter-Lumi™ Assay Kit (Beyotime, China). Cells were cultured at a density of 5000 cells/cm² in 96-well cell culture plates. After red light irradiation, the cells were

cultured for 48 h and washed with PBS. The cells were treated with an ATP assay kit and ATP levels were detected through chemiluminescence using an automatic microplate reader (Synergy H1, Agilent BioTek, USA).

2.6 Co-culture

ECs and SMCs were stained using CellTracker™ Green CMFDA Dye and CellTracker™ Red CMTPX Dye (Thermo, USA), respectively, and then seeded on 24-well cell culture plates at a density of 10000 cells/well (total 20000 cells/well). After exposure to red light, the cells were co-cultured for 48 h. At least 9 fluorescence micrographs were taken to determine the cell density (Ti2, Nikon, Japan).

2.7 ECs NO assay

NO production in ECs was detected using an NO fluorescent probe (BBoxiProbe O36, BestBio, China). ECs were cultured at a density of 5000 cells /cm². After light exposure, the cells were cultured for 48 h and washed with PBS. Then, the cells were incubated with the NO fluorescent probe (diluted with phenol red-free DMEM medium) for 50 min. The fluorescence intensity of NO was detected by the automatic microplate reader at 490/525 nm.

2.8 Cell immunofluorescence staining

Cells were fixed with 4% paraformaldehyde in PBS 48 h post-red light PBM treatment. 0.1% Triton X-100 of TBS was used for intracellular antigen staining to permeabilize the cell membrane. The cells were incubated with 0.1% BSA of TBS buffer solution at room temperature for more than 1 h to bind the non-specific site and then were incubated with antibodies for 16 h at 4 °C. Rabbit anti-VEGF (A12303, ABclonal, China) and rabbit anti-CD31 (11265-1-AP, Proteintech, China) antibodies were used to mark the angiogenesis of ECs. Mouse anti-OPN (14-9096-82, Invitrogen, USA), rabbit anti-calponon1 (ab46794, Abcam, UK) and mouse anti-αSMA (A5228, Sigma, USA) antibodies were used to mark the phenotypic transition of SMCs. After incubation with primary antibodies, the samples were washed at least three times with PBS. Then Alexa Fluor 568-labeled goat anti-rabbit IgG or 568-labeled goat anti-mouse IgG (Invitrogen, USA) with DAPI (Sigma, USA) were applied for 1 h at room temperature in the dark. Fluorescence images of samples were observed under a confocal laser scanning microscope (Zeiss LSM900).

2.9 SMC Ca^{2+} assay

The Ca^{2+} content in SMCs was detected using a Fluo-4 Calcium Assay Kit (Beyotime, China). After exposure to light, the cells were cultured for 48 h and washed with PBS. The cells were incubated with calcium fluorescent probe (diluted with FBS-free DMEM medium) for 30 min. Finally, the fluorescence intensity of Ca^{2+} was detected by the automatic microplate reader at 490/525 nm.

2.10 Western blot and qPCR tests

Cells were harvested and centrifuged 48 h post light exposure for further experimentation. Western blot (WB) and qPCR analyses were outsourced to Newbe Biology (Hangzhou, China). Antibodies used in WB included: p-eNOS (PA5-104858, Invitrogen, USA), eNOS (32027, Cell Signaling Technology, USA), endothelin 1 (12191-1-AP, Proteintech, China), angiotensin II (ab286174, Abcam, UK), p-MLC (3671, Cell Signaling Technology, USA), MLC (ab92721, Abcam, UK), RhoA (ab187027, Abcam, UK), ROCK (21850-1-AP, Proteintech, China), PLC (ab302940, Abcam, UK), VE-cadherin (36-1900, Invitrogen, USA), ZO-1 (40-2200, Invitrogen, USA), PTGIS (ab23668, Abcam, UK), and thrombomodulin (14318-1-AP, Proteintech, China), β-actin (ab8266, Abcam, UK).

2.11 Rat abdominal aorta model

Sprague–Dawley (SD) rats (male, weighing 350-400 g) were obtained from the Zhejiang Center of

Laboratory Animals (ZJCLA, Hangzhou, China). All animal experiments were approved by the Institutional Animal Care and Use Committee (IACUC), ZJCLA (approval number ZJCLA-IACUC-20011136).

Balloon-mediated vascular injury was induced in the abdominal aorta of the SD rats. The rats were anesthetized by isoflurane inhalation (5% for induction, then 1.5% for maintenance). A longitudinal incision was made and the abdominal aorta was dissected. A 1.75 mm diameter side-firing fiber balloon (MATRIXMEDICAL, Hangzhou, China) was inserted into the abdominal aorta, inflated with purified water under hydraulic pressure to 4 atm, and kept at this pressure for 3 min. As disclosed in the manufacturer's patent (CN120203754A), the light-emitting component could be driven to move relative to the balloon body (axially or rotationally), which improved the uniformity of light distribution over the injured area. For the PBM treated group, a red light fiber in the balloon was activated to provide 20 mW/cm² irradiation for 3 mins. Irradiance was measured using a calibrated power meter placed directly at the outer surface of the inflated balloon, which corresponds to the vessel-wall interface during in vivo treatment. After the deflation and withdrawal of the balloon, the surgical site was closed with sutures. No anticoagulation or antiplatelet treatments were given before and after the surgeries. At 3 days or 21 days later, rats were anesthetized, and the abdominal aortas were harvested for analysis.

2.12 Histological staining

Vascular samples were fixed with 4% paraformaldehyde at room temperature overnight and the fixed samples were embedded in paraffin and sectioned. Slides were then stained with hematoxylin and eosin (H&E) to observe sample morphology.

2.13 Tissue immunofluorescence staining

Tissue sections were first blocked with 3% bovine serum albumin (BSA, Sigma-Aldrich, USA) solution for 30 min and then incubated with the following primary antibodies in BSA solution overnight at 4 ℃: Anti-CD68 (HKA50068, HaoKe, China), iNOS (HKA50053, HaoKe, China), CD206 (18704-1-AP, Proteintech, China), CD31 (ab182981, Abcam, UK), VEGF (A12303, ABclonal, China), Cyclin D1 (BX50071, Biolynx, China), PCNA (10110S, Cell Signaling Technology, USA) and α-SMA (HKA50059, HaoKe, China). After that, samples were washed with PBS and incubated with goat anti-rabbit secondary antibody or goat anti-mouse antibody for 1 h at room temperature. Nuclei were counterstained with DAPI. The stained samples were scanned with a fluorescence microscope (Nikon).

2.14 Statistical analysis

All data were obtained from at least three parallel samples per condition in each experiment and are expressed as mean ± standard deviation (SD). A normality test was applied. Statistical significance between different groups was assessed using one-way ANOVA followed by Tukey's post hoc test. The minimum significance level was set at $*p < 0.05$, $**p < 0.01$ and $***p < 0.001$.

3 Results

3.1 Enhancement of EC migration and proliferation by PBM

During cell experiments, we used the surface light source of LEDs for illumination and measured the temperature changes. We found that the changes in temperature were not drastic (Fig. S1), so temporarily we did not take the impact of temperature into detailed consideration. To investigate the effect of red light on EC migration, we performed scratch assays and assessed the migration ratio 6 h and 24 h post-irradiation. The scratch width was narrower in the red light group than in the control group (Fig. 2a). The 3.6-7.2 J/cm² PBM groups exhibited superior migration capabilities relative to the control group and the migration ratio increased significantly from 22% ± 4% in the control group to 39% ± 8% in the 3.6 J/cm² PBM group and 38% ± 7% in the

7.2 J/cm² PBM group (Fig. 2b).

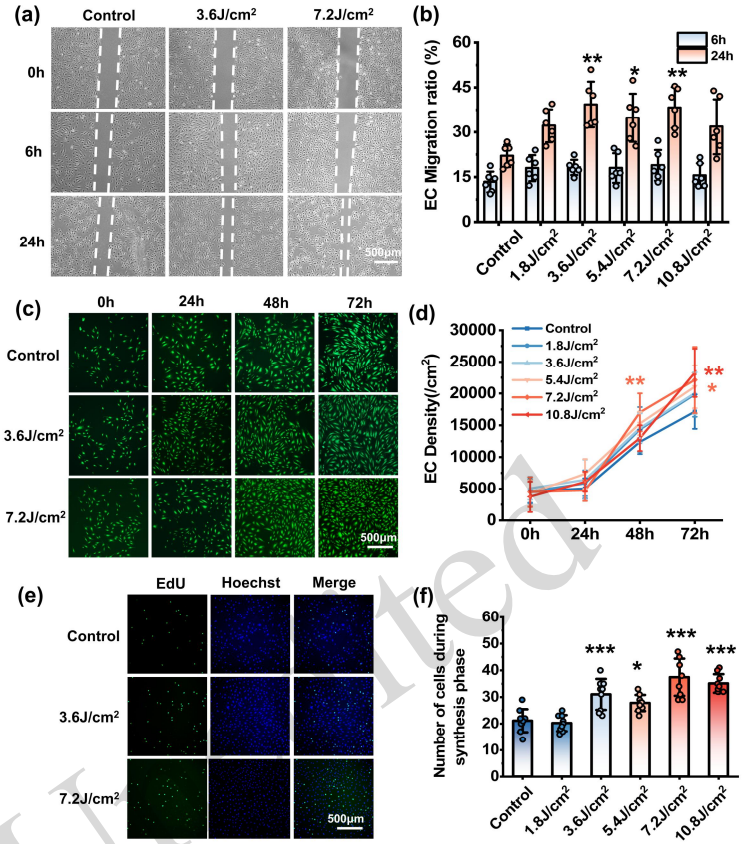

Fig. 2 The effect of PBM on EC migration and proliferation capacities. (a) Endothelial cell migration under 0, 3.6, or 7.2 J/cm² irradiation. (b) The migration ratio of ECs 6 h and 24 h after red light phototherapy; data are mean ± SD (n = 6). (c) Endothelial cell proliferation under 0, 3.6, and 7.2 J/cm² irradiation. (d) Density of ECs 0, 24, 48, and 72 h post different dose irradiation; data are mean ± SD (n = 10). (e) EdU staining of ECs 24 h post irradiation. (f) Number of ECs during synthesis phase; data are mean ± SD (n = 9). *p < 0.05, **p < 0.01, ***p < 0.001 versus the control groups. P values were determined using one-way ANOVA with Tukey's post hoc analysis.

Given that EC proliferation is a hallmark of angiogenesis and tissue repair, we assessed the cell proliferation situation after PBM (Fig. 2c). The number of ECs 48 h post 7.2 J/cm² red light irradiation increased moderately from $1.24 \pm 0.19 \times 10^4$ cells/cm² to $1.70 \pm 0.30 \times 10^4$ cells/cm². After 72 h, the number of ECs was $2.33 \pm 0.38 \times 10^4$ cells/cm² under 10.8 J/cm² irradiation, higher than the control group (Fig. 2d). The number of cells during the synthesis phase, labeled by the incorporation of EdU, also increased after PBM (Fig. 2e, f), following a similar trend to the proliferation experiment. Additionally, ATP production by mitochondria was slightly enhanced after receiving PBM treatment. The ATP levels in ECs was enhanced by 33% ± 29% under 7.2 J/cm² irradiation (Fig. S2a), indicating slightly improved cell viability. Genes related to cell proliferation and migration ability such as Rac1 (Ma et al., 2023), PDGF (Zymek et al., 2006), EGFR (Cheng et al., 2021), and Fn1(Cai et al., 2018) exhibited slight dose-dependent increases in expression levels (Fig. S2b).

The above results showed that red light modulation can enhance the migration and proliferation of endothelial cells to some extent, consistent with previous findings (Oh et al., 2018). The effect of PBM seems dose-dependent: when the dose is small, the effect is weak and modest. The increase in viability of ECs can directly accelerate the process of intima injury repair. If quickly covering the damaged area, ECs are able to quickly form a complete inner layer, reducing platelet adhesion and aggregation, thereby reducing the risk of thrombosis. These observations raise the possibility that PBM may offer a useful experimental strategy for further investigation in the context of vascular injury.

3.2 Inhibition of SMC proliferation by PBM

SMCs also play a pivotal role in the pathogenesis of vascular injury repair. PBM had no significant effect on SMC migration ability (Fig. S3). After 24 h, the scratches in all experimental groups had almost healed. However, for proliferation, red light modulation inhibited the growth of SMCs (Fig. 3a). The inhibitory effect of red light on SMCs increased with increasing irradiation dose. The number of SMCs increased to 1.88 ± 0.14 $\times 10^4$ cells/cm² after 72 h without light treatment, but reduced to 1.43 ± 0.21 $\times 10^4$ cells/cm² after 5.4 J/cm² irradiation, 1.36 ± 0.30 $\times 10^4$ cells/cm² after 7.2 J/cm² irradiation, and 1.25 ± 0.40 $\times 10^4$ cells/cm² after 10.8 J/cm² irradiation (Fig. 3b). By slowing down the proliferation rate of SMCs, the occurrence of intimal hyperplasia may be reduced, thereby maintaining the patency of blood vessels.

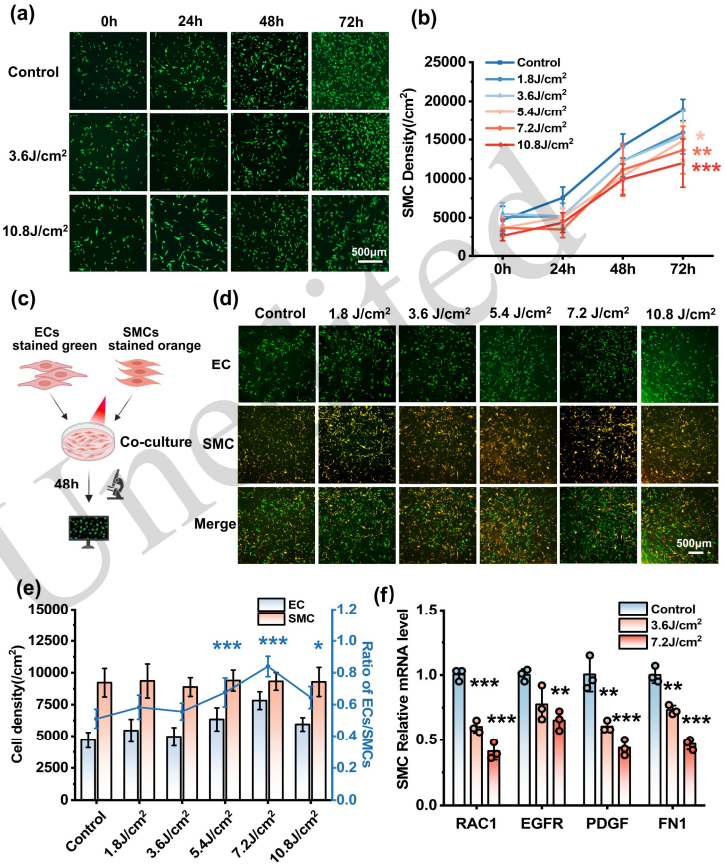

Fig. 3 The effect of PBM on smooth muscle cell (SMC) proliferation capacity and EC/SMC co-culture. (a) SMC proliferation under 0, 7.2, and 10.8 J/cm² irradiation. (b) Cell density of SMCs 0, 24, 48, and 72 h post different dose irradiation; data are mean ± SD (n = 10). (c) Schematic of the co-culture evaluation of ECs/SMCs. (d) Co-culture of ECs and SMCs treated with different irradiation doses (green: ECs, orange: SMCs). (e) Quantification of the cell density and the ratio of ECs/SMCs; data are mean ± SD (n = 9). (f) Intracellular RNA expression level of Rac1, EGFR, PDGF and Fn1 in SMCs after different irradiation treatments; data are mean ± SD (n = 3). * p < 0.05, * * p < 0.01, * * * p < 0.001 versus the control groups. P values were determined using one-way ANOVA with Tukey's post hoc analysis.

In addition, the results of the co-culture experiment (Fig. 3c) indicated that the EC/SMC ratio could be improved after red light irradiation, especially when the exposure dose was above 5.4 J/cm². The number of ECs in co-culture after PBM was gradually increased. The EC/SMC ratio was raised to 0.68 ± 0.09 after receiving 5.4 J/cm² irradiation and 0.84 ± 0.06 after receiving 7.2 J/cm² irradiation, but was only 0.51 ± 0.06 without PBM (Fig. 3 d-e). Furthermore, the qPCR results of Rac1, PDGF, EGFR, and Fn1 genes related to cell growth and migration showed that these genes had lower expression after PBM, which may result in inhibition of SMCs. Specifically, under 3.6 J/cm² and 7.2 J/cm² irradiation, the expression of Rac1 in SMCs was reduced by 40% ±

5% and 59% ± 6%, respectively, while PDGF was reduced by 40% ± 4% and 56% ± 6%, EGFR by 23% ± 13% and 35% ± 8%, and Fn1 by 27% ± 4% and 53% ± 4% (Fig. 3f). High dose PBM may suppress SMC proliferation and mobility viability by downregulating the expression of these key genes. However, in terms of cell morphology, we did not observe changes in either ECs or SMCs after PBM treatment (Fig. S4, Fig. S5). Our results indicated that red light therapy could depress SMC proliferation and promote the competitive growth of ECs over SMCs, which is beneficial for the regeneration of endothelium and reducing the risk of restenosis.

3.3 Promotion of NO release and angiogenesis in ECs by PBM

NO is a crucial biological signaling molecule which plays an important role in various physiological and pathological processes in the human body, including angiogenesis and vasodilation (Caldwell et al., 2003). Vascular endothelial growth factor (VEGF) is a potent angiogenic factor, playing a critical role in both physiological and pathological angiogenesis (Fukumura et al., 2001). Aiming to investigate the effect of PBM therapy on angiogenesis, we detected the expression of NO, VEGF and platelet endothelial cell adhesion molecule-1 (CD31) in ECs (Fig. 4a). After light irradiation, the release of NO was increased by 30% when the dose was 5.4 J/cm² or 10.8 J/cm², compared to control group (Fig. 4b, e). Immunofluorescence of VEGF expression increased by about 50% when the dose was 5.4 -10.8 J/cm² (Fig. 4c, f). PBM also increased the expression of CD31. When the dose was 10.8 J/cm², the maximum increase was 101% ± 19%, which was beneficial for endothelium regeneration (Fig. 4d, g). Up-regulation of VEGF and CD31 would be conducive to the remodeling of blood vessels, enhancing the adhesion and signal transduction between ECs, thereby accelerating angiogenesis.

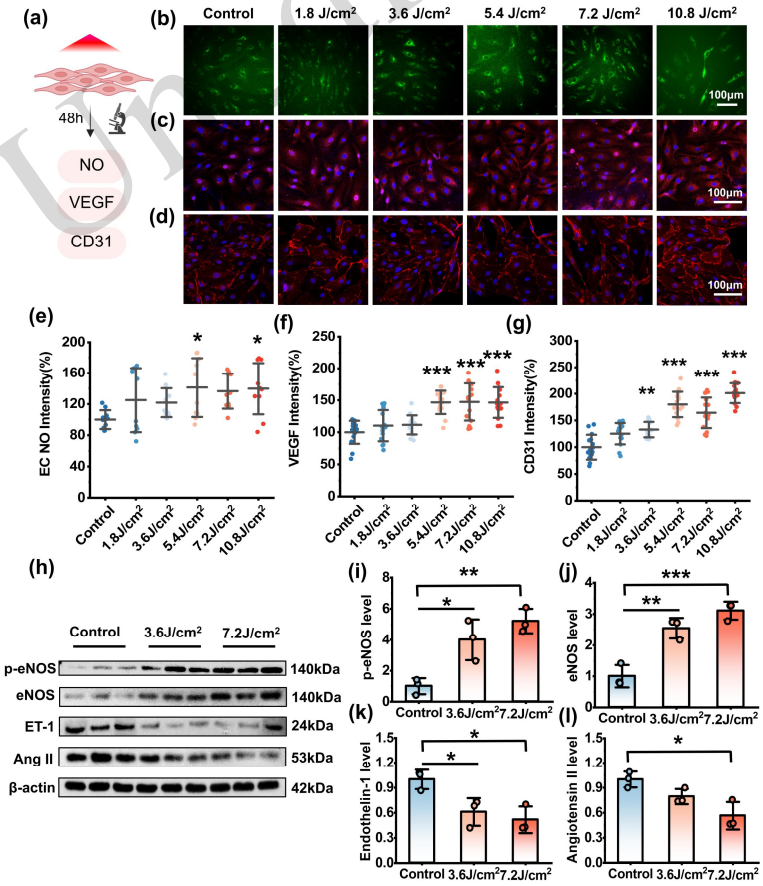

Fig. 4 The effect of PBM on vascular regeneration and dilation in ECs. (a) Schematic of the in vitro evaluation of endothelial functions. (b) NO expression in ECs with different irradiation doses. (c) VEGF expression in ECs with different irradiation doses (bule: DAPI, red: VEGF). (d) CD31 expression in ECs with different irradiation doses (bule:

DAPI, red: CD31). (e) Quantification of NO expression; data are mean ± SD (n = 10). (f) Quantification of VEGF expression; data are mean ± SD (n = 15). (g) Quantification of CD31 expression; data are mean ± SD (n = 15). (h) Representative WB bands of p-eNOS, eNOS, ET-1 and Ang II proteins in ECs after PBM. For WB quantitative data (i-l), data are mean ± SD (n = 3). *p < 0.05, **p < 0.01, ***p < 0.001 versus the control groups. P values were determined using one-way ANOVA with Tukey's post hoc analysis.

Balloon angioplasty poses a risk of vasospasm due to mechanical stimuli causing excessive contraction of vascular smooth muscle and endothelial dysfunction (Wong et al., 2005; Yasue et al., 2008). p-eNOS is the pivotal molecule for ECs to physiologically produce NO which is involved in the regulation of basal vascular tone in humans (Lin et al., 2022). The results of WB analysis confirmed that red light modulation promoted the expression of p-eNOS and eNOS in ECs. The expression of p-eNOS increased by 3 to 4 times after PBM, while eNOS expression increased by 155% ± 33% under 3.6 J/cm² irradiation and 211% ± 29% under 7.2 J/cm² irradiation (Fig. 4h-j), reflecting the activation of NOS. The expression of endothelin 1 and angiotensin II, which are potent vasoconstrictors and proliferators of SMCs, was downregulated after PBM due to the increase of NO. Endothelin 1 expression decreased by 39% ± 17% under 3.6 J/cm² irradiation and 48% ± 14% under 7.2 J/cm² irradiation while angiotensin II was reduced by 21% ± 9% and 44% ± 17% (Fig. 4k, l). The increase in NO release and the reduced vasoconstrictor expression suggest that photobiological regulation may have potential relevance for modulating vascular tone, although this remains to be tested in functional models.

3.4 Downregulation of SMC synthetic phenotype and contractility by PBM

Vascular SMCs exhibit strong phenotypic plasticity, including contractile and synthetic phenotypes which are characterized by their morphology, proliferation and migration rates, and the expression of different hallmark proteins (Rensen et al., 2007). Having observed that red light regulation reduced the proliferation rate of SMCs, we then investigated whether the downregulation of the proliferation rate was associated with the phenotypic transition of cells. We labeled cells with calponin, α-SMA (a marker protein of the contractile phenotype) and osteopontin (OPN, a marker protein of the synthetic phenotype) (Fig. 5a). Combining the immunofluorescence images of CNN1 and α-SMA, the effect of PBM on the contraction phenotype was not significant, but showed a slight promotion (Fig. 5b, e, Fig. S6). However, red light modulation inhibited the expression of OPN, with a decrease of 23% ± 12% even at the lower irradiation dose of 1.8 J/cm². The decrease in OPN expression was positively correlated with the increase of irradiation dose. When the dose was 5.4 J/cm² or 7.2 J/cm², the expression was decreased by about 50%. When the dose was 10.8 J/cm², the maximum decrease was 62% ± 9%, which was beneficial for inhibiting SMC proliferation and reducing the restenosis ratio (Fig. 5c, f).

In addition to reducing the synthetic phenotype of SMCs, PBM tends to reduce their contractile ability while simultaneously maintaining the contractile phenotype. Vascular smooth muscle cell (VSMC) hypercontractility is dependent on the cytoplasm Ca^{2+} sensitivity or the quantity of Ca^{2+} ions. After red light modulation, the concentration of calcium ions in the SMCs was decreased by 13% ± 9% under 5.4 J/cm² irradiation and 23% ± 17% under 10.8 J/cm² irradiation (Fig. 5d, g). Calcium functions by binding with calmodulin (CaM). The Ca^{2+}-CaM complex then directly activates the myosin light chain kinase (MLCK) to phosphorylate the myosin light chain, triggering the contraction of SMCs (Kim, 2016; Yi et al., 2019). Excessive constriction may cause vasospasm. Contraction and relaxation of vascular smooth muscle are regulated by MLCK and myosin light chain phosphatase (MLCP) through phosphorylation and dephosphorylation of MLC (Injeti et al., 2008). Phosphorylated myosin light chain (p-MLC) also decreased after PBM with reductions of 20% ± 10% under 3.6 J/cm² irradiation and 43% ± 16% under 7.2 J/cm² irradiation, while the expression of MLC remained unchanged (Fig. 5h-j). We hypothesized that red light modulation could regulate the Ca^{2+} concentration and MLC phosphorylation level by affecting the activity of their regulatory pathways such as RhoA/ROCK (Nohria et al., 2006; Kato et al., 2012) and PLC/PKC (Nakano et al., 2002). ROCK/Rho-kinase inhibits MLCP, leading to augmentation of MLC phosphorylation and Ca^{2+} sensitization (Shimokawa et al., 2005). Red light modulation downregulated the expression of RhoA by 20% ± 10% under

3.6 J/cm² irradiation and 39% ± 8% under 7.2 J/cm² irradiation (Fig. 5k). ROCK was also decreased by 25% ± 10% and 47% ± 14% (Fig. 5l). The phospholipase C (PLC) activity, which was positively correlated with the contractility, was reduced by 24% ± 10% and 44% ± 14% under 3.6 and 7.2 J/cm² irradiation, respectively (Fig. 5m). PLC can hydrolyze 4, 5-diphosphate phosphatidylinositol (PIP2) to 1, 4, 5-triphosphate inositol (IP3) which can bind to the IP3 ligand calcium channel on the endoplasmic reticulum Thus, the deactivation of PLC inhibited the calcium channel, reducing the intracellular Ca^{2+} concentration. Reducing the Ca^{2+} concentration and p-MLC attenuates the contractile responsiveness and sensitivity of arteries, therefore red light treatment may have potential application in reducing excessive contraction of SMCs which may result in vasospasm and myocardial ischemia.

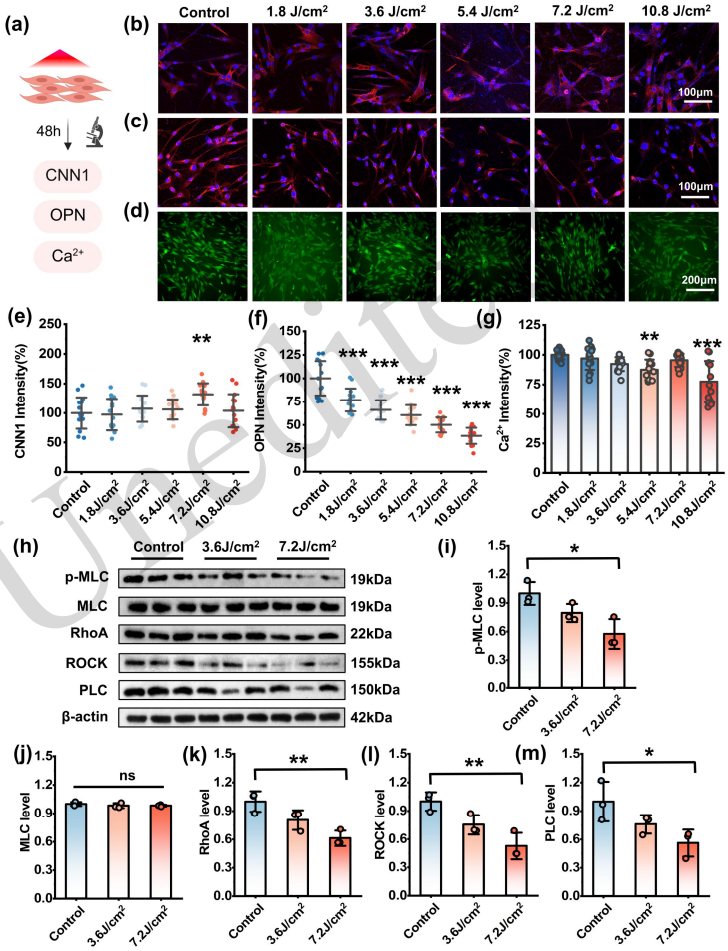

Fig. 5 The effect of PBM on phenotypic transformation and cell contraction in SMCs. (a) Schematic of the in vitro evaluation of SMC functions. (b) CNN1 expression in SMCs with different irradiation doses (bule: DAPI, red: CNN1). (c) OPN expression in SMCs with different irradiation doses (bule: DAPI, red: OPN). (d) Intracellular Ca^{2+} with different irradiation doses. (e) Quantification of CNN1 expression; data are mean ± SD (n = 15). (f) Quantification of OPN expression; data are mean ± SD (n = 15). (g) Quantification of intracellular Ca^{2+}; data are mean ± SD (n = 15). (h) Representative WB bands showing changes in the levels of p-MLC, MLC, RhoA, ROCK and PLC proteins in SMCs after PBM. For WB quantitative data (i-m), data are mean ± SD (n = 3). *p < 0.05, **p < 0.01, ***p < 0.001 versus the control groups. P values were determined using one-way ANOVA with Tukey's post hoc analysis.

3.5 Promotion of intimal repair after arterial injury in rats by PBM

Aiming to evaluate the in vivo repair ability of PBM, rats were subjected to balloon-mediated abdominal aorta injury, which is a well-established mimetic surgical model for balloon angioplasty. In the rat model, a

balloon with a built-in red light optical fiber was used to give 3.6 J/cm² PBM therapy. We assessed the effects of PBM on the inflammatory microenvironment 3 and 7 days post vascular injury and evaluated the reparative effects of PBM on the injured arteries on day 21 (Fig. 6a).

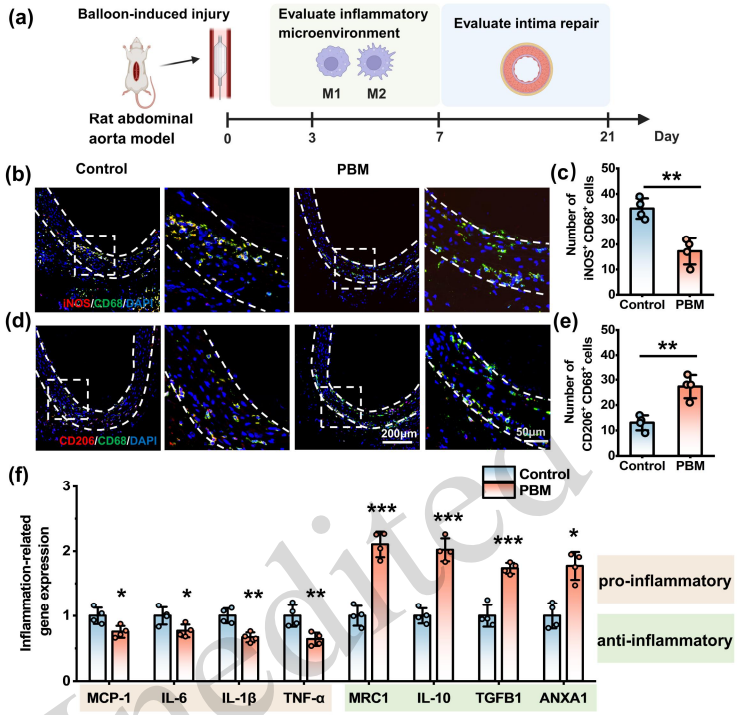

Fig. 6 The effects of PBM on macrophage infiltration and inflammation 3 days after balloon injury. (a) Schematic illustrating balloon dilation in the rat abdominal aorta model. (b) Representative iNOS (red) and CD68 (green) double staining of aortas from different groups. Regions outlined in white are expanded. (c) Corresponding quantification of the numbers of iNOS⁺ CD68⁺ cells (n = 4). (d) Representative CD206 (red) and CD68 (green) double staining of aortas from different groups. Regions outlined in white are expanded. (e) Corresponding quantification of the numbers of CD206⁺ CD68⁺ cells (n = 4). (f) RNA expression of inflammation-related genes (n = 4). ∗p < 0.05, ∗∗p < 0.01, ∗∗∗p < 0.001 versus the control groups. P values were determined using one-way ANOVA with Tukey's post hoc analysis.

Controlling inflammation levels after vascular injury in the early stages is crucial for reducing vascular restenosis because inflammation will accelerate the proliferation and migration of SMCs and delay endothelial healing. Therefore, it is essential to evaluate the regulatory role of PBM in the early-stage inflammatory microenvironment of vascular injury. Immunofluorescent co-staining was conducted on rat vessels 3 days after vascular injury to observe the total macrophage marker CD68, pro-inflammatory macrophage marker iNOS and anti-inflammatory macrophage marker CD206. Three days after vascular injury, we found there was a significant reduction in the number of iNOS⁺ and CD68⁺ cells in the PBM groups compared to the control group (Fig. 6b, c). Treatment with PBM also increased the number of CD206⁺ and CD68⁺ cells compared to the control group (Fig. 6d, e). This shows that PBM treatment reduced the number of pro-inflammatory M1 macrophages while increasing the number of anti-inflammatory M2 macrophages. The qPCR results from PBM treatment also supported the downregulation of the expression of pro-inflammatory genes (such as MCP-1, IL-6, IL-1β, TNF-α) in injured vessels and the upregulation of anti-inflammatory genes like MRC1, IL10, TGFB1 and ANXA-1. The expression of anti-inflammatory genes nearly doubled (Fig. 6f). The above results indicate that PBM treatment showed superior efficacy in attenuating the inflammatory response in injured vessels to inhibit neointimal hyperplasia. Also, H&E staining showed that the vessels were not narrowed on day 3 (Fig. S7). Seven days after balloon injury, the reduced inflammation could still be observed (Fig. S8a). The control group showed mild intima hyperplasia and SMC proliferation 7 days after the injury (Fig. S8b, c), but in the

PBM group the intima began to heal, according to images from CD31 staining (Fig. S8d, e).

Next, the reparative effects of PBM on injured arteries were investigated on day 21. Color Doppler ultrasound showed there was no significant difference in blood flow velocity between the control groups and the PBM treatment group (Fig. S9). Subsequently, the reparative effects of PBM were assessed through histological analysis. H&E staining was used to evaluate the intima and media of the rat aorta abdominalis (Fig. 7a). Unsurprisingly, neointimal hyperplasia was observed in the control group. After PBM treatment, the intima thickness was reduced about 38 μm (Fig. 7b) while the thickness of the media remained unchanged (Fig. 7c). The intima/media ratio decreased from 0.70 ± 0.13 to 0.22 ± 0.13 (Fig. 7d). Post-hoc power analysis of the intima/media ratio data (two-tailed independent t-test) showed power for n = 4 per group reached 98%. Then we detected CD31 and VEGF, which play an important role in EC regeneration (Fig. 7e). The results of immunofluorescence staining showed that their expression nearly doubled after receiving PBM (Fig. 7f), which would contribute to restoring the original physiological structure. To further characterize the recovery of endothelial function, we selected some proteins for testing. After receiving PBM treatment, the expression of p-eNOS was elevated by 162% ± 24%, VE-Cadherin by 90% ± 35%, ZO-1 by 54% ± 9%, PTGIS by 159% ± 17%, and thrombomodulin by 109% ± 54% (Fig. 7g-m). This indicated that PBM seems to be helpful in improving re-endothelialization, vascular permeability and thrombosis resistance after balloon injury.

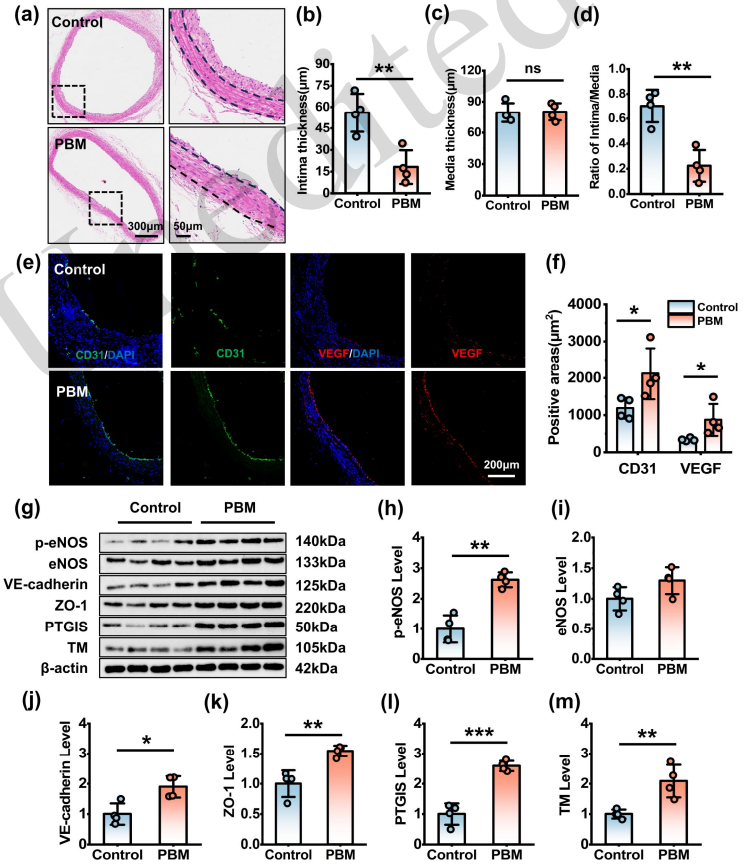

Fig. 7 The effects of PBM on intima repair 21 days after balloon injury. (a) H&E staining of rat aortas. (b) Quantification of average intima thickness (n = 4). (c) Quantification of media thickness (n = 4). (d) Quantification of intima/media ratios (n = 4). (e) Representative immunofluorescent images of CD31 and VEGF in different groups. (f) Corresponding quantification of the positive areas of CD31 and VEGF (n = 4). (g) Representative WB bands showing changes in the levels of p-eNOS, eNOS, VE-cadherin, ZO-1, PTGIS and TM proteins in rat artery after PBM. For WB quantitative data (h-m), data are mean ± SD (n = 4). *p < 0.05, **p < 0.01, ***p < 0.001 versus the control groups. P values were determined using one-way ANOVA with Tukey's post hoc analysis.

In response to vascular injury, contractile wound SMCs switch to synthetic SMCs, which exhibit an increased proliferation capacity contributing to neointimal formation. Two typical proliferative markers, PCNA and Cyclin D1, were highly expressed in the neointimal areas of the aortas in the control groups with co-expression of an SMC marker, α-SMA (Fig. 8a-d). In contrast, there were fewer $PCNA^+$ α- SMA^+ and Cyclin $D1^+$ α- SMA^+ cells in the PBM group. PBM was associated with reducing the possibility of restenosis in the rat model but whether this translates to reduced restenosis in humans remains to be determined.

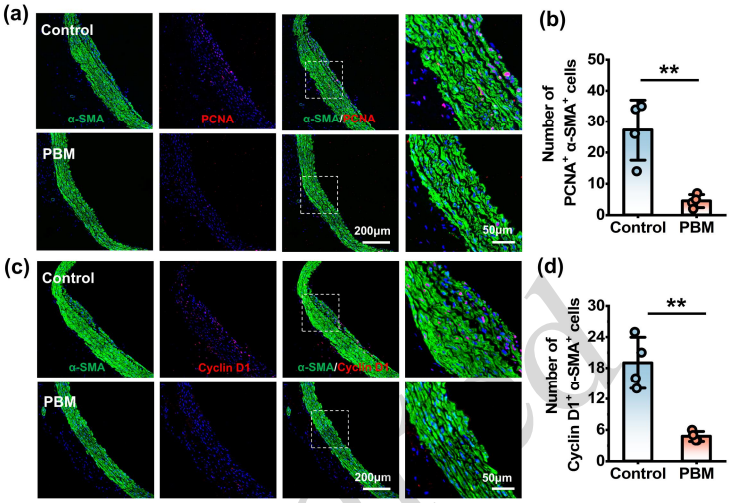

Fig. 8 The effects of PBM on smooth muscle cell proliferation 21 days after vascular balloon injury. (a) Representative PCNA (red) and α-SMA (green) double staining of aortas from different groups. Regions outlined in white are expanded. (b) Corresponding quantification of the numbers of $PCNA^+$ α-SMA^+ cells (n = 4). (c) Representative Cyclin D1 (red) and α-SMA (green) double staining of aortas from different groups. Regions outlined in white are expanded. (d) Corresponding quantification of the numbers of Cyclin $D1^+$ α-SMA^+ cells (n = 4). ∗p < 0.05, ∗∗p < 0.01, ∗∗∗p < 0.001 versus the control groups. P values were determined using one-way ANOVA with Tukey's post hoc analysis.

4 Discussion

Current antiproliferative therapies for post-angioplasty restenosis reduce neointimal hyperplasia but delay endothelial healing, increasing the risk of late thrombosis and restenosis. This trade-off highlights the need for alternative strategies. This proof-of-concept study provides preliminary evidence that PBM, a non-pharmacological light-based approach, is associated with markers of vascular repair after balloon injury. The findings raise the possibility of a shift from an inhibitory toward a restorative paradigm, but this interpretation remains speculative and requires confirmatory studies.

Red-light PBM has been shown to directly affect ECs. Schindl et al. (2003) reported that 670 nm PBM promotes HUVEC proliferation. Subsequent studies demonstrated that PBM at 650 nm enhances HUVEC proliferation, migration, and tube formation via the PI3K/Akt and VEGFA/VEGFR2/STAT3 pathways, accompanied by increased HIF-1α and eNOS expression, while the MAPK/ERK pathway fine-tunes these responses (Zhang et al., 2022). Consistent with previous reports, we observed that PBM promoted EC migration, proliferation, NO release, and key protein expression (such as VEGF, CD31, p-eNOS) to a certain extent, consistent with previous studies. It also concurrently suppressed VSMC proliferative and contractile capacities, exhibiting potential application in vascular repair. PBM acts sequentially: direct photophysical actions on chromophores, then downstream signaling cascades and finally proteomic remodeling, phenotypic adaptation, proliferation, and migration. Our experimental design captures mainly the subsequent effect (24 h and 48 h for most endpoints) from a long cascade of downstream events. Primary effects were not directly measured, which may explain why we observed only modest and variable ATP changes - the initial bioenergetic peak occurs

within minutes after irradiation and had already dissipated by the time of our measurement. The mechanism of PBM is highly complex, and the Cox mechanism may not fully explain it. For example, the significant increase in p-eNOS we observed may be related to the activation of NOS (Pope and Denton, 2023; Balbi et al., 2025). Furthermore, recent work showed irradiation can drive metabolic switches (stimulating oxidative phosphorylation), refining the understanding of the bioenergetic dynamics of PBM (Amaroli et al., 2019).

Most studies have been conducted with light in the red or infrared spectrum. However, increasing evidence shows that shorter wavelengths may also support tissue regeneration processes (Bayat et al., 2022). Light can trigger the release of the the important mediator NO by dissociating it from its binding sites. This release occurs in a wavelength-dependent manner. Adamskaya et al. (2011) compared the effects of different wavelengths and found blue light was more potent in reducing wound size and enhancing epithelialization in an excision model. Apart from wavelength, the effect of light efficiency may also be related to the lighting mode. Some studies demonstrated that a pulsed wave (PW) mode may be more advantageous than a continuous wave (CW) mode, particularly in wound healing and stroke management (Joensen et al., 2012). The type of light source is also a key point. Compared to lasers, the broader spectral bandwidth of LEDs may alter the efficiency and selectivity of cytochrome c oxidase activation (Pruitt et al., 2022). Furthermore, the higher beam divergence of LEDs leads to more rapid decay of irradiance with tissue depth compared to collimated laser beams, potentially shifting the effective therapeutic window (Heiskanen and Hamblin, 2023; Salehpour et al., 2023). Therefore, in terms of the effects of light wavelength and light mode on the repair of the endothelium, there is still some room for exploration in the future to further enhance therapeutic efficacy.

In this study, we selected a dose of 3.6 J/cm² as the treatment dose for the animal experiments. This dose falls within the range previously reported to be effective in some studies, which ranges from about 1 to 5 J/cm² (Selestin et al., 2024). Doses significantly higher than a safe range may induce biphasic dose responses where the beneficial effects are diminished or even replaced by inhibitory effects. This research was more of an exploratory study. It provided proof-of-concept that a proper dose derived from in vitro screening elicits detectable effects in vivo. Whether an optimal dose exists, and what it might be, remains to be determined in a dedicated dose-finding study, which we have now clearly proposed as the next step.

However, there is still a considerable distance to go before this treatment approach can be clinically applied. HUVECs are venous in origin, while arterial balloon angioplasty targets arterial endothelium. Venous and arterial endothelial cells differ in eNOS expression, shear stress response, and inflammatory regulation. Therefore, our findings require validation in arterial EC lines. Simple EC and SMC experiments are unable to fully demonstrate the vascular microenvironment. While this study demonstrates some efficacy of PBM therapy in attenuating the development of neointimal hyperplasia at early and intermediate time points, a limitation of this work is the absence of long-term outcome data. Restenosis is a chronic process, and the long-term durability of the therapeutic effect, beyond the peak of SMC proliferation, warrants further investigation. Future studies using extended observation periods (90 or 180 days) in larger animal models are essential to confirm the sustained suppression of neointimal growth, the persistence of a functional endothelium, and the long-term safety profile of this approach. Randomization, blinding, and group sizes are needed to ensure reproducibility and robustness in animal models but full blinding was difficult in this specific model due to the nature of the surgical and PBM procedures. The failure to implement double-blindness is also an aspect of this study that could be improved. The present model uses a mechanical injury in healthy normolipidemic rats, which does not recapitulate complex atherosclerotic, diabetes, or dyslipidemia situations. Direct extrapolation to clinical angioplasty is not proper without further testing in disease-relevant models. Including pharmacological controls such as NO donors, drug-coated balloons or stents would provide a valuable benchmark for the potency of the PBM effect. A direct comparison between PBM and current clinical standards is a critical next step for our research.

5 Conclusions

This research provides preliminary evidence that may inform future development of balloon-based therapeutic strategies. PBM promoted EC migration, proliferation, NO release, and CD31 expression, while concurrently suppressing VSMC proliferative and contractile capacities. It showed that PBM treatment has potential application in enhancing intima repair and reducing vasospasm after balloon injury. Rat model outcomes confirmed PBM attenuated the vascular inflammation reaction and reduced neointimal hyperplasia. These findings suggest that PBM shows promise as a potential approach for mitigating neointimal hyperplasia, though further validation is required.

Declaration of interests

The authors declare no conflicts of interest in the publication of in this paper.

Data availability statement

Primary data in this study are available from the author upon request.

Acknowledgments

This research was supported by the Key Research and Development Program of Zhejiang Province (2024C03076), the Opening Foundation of the State Key Laboratory of Transvascular Implantation Devices (QZ3812202404), and the Foundation of Transvascular Implantation Devices Research Institute (TIDRI) (KY012025003, KY012024008).

Author contributions

Conceptualization, P.J., K.R., Y.W. and J.J.; methodology, S.J., K.R.; validation, S.J., K.R.; investigation, S.J. and X.W.; resources, P.J., Y.P., K.R. and Y.W.; data curation, X.W. and Y.Y.; writing – original draft, S.J.; writing – review & editing, K.R. and Y.W.; visualization, S.J. and C.Y.; supervision, K.R., Y.W. and J.J.; project administration, K.R.; funding acquisition, K.R and J.J..

Compliance with ethics guidelines

All animal experiments were approved by the Institutional Animal Care and Use Committee (IACUC), the Zhejiang Center of Laboratory Animals. The approval number for these experiments was ZJCLA-IACUC-20011136.

Declaration on the use of generative AI tools

During the preparation of this work, the authors used DeepSeek in order to improve language and readability, check for grammatical errors. After using this tool/service, the authors reviewed and edited the content as needed and take full responsibility for the content of the publication.

References

Tsao C W, Aday AW, Almarzooq Z I, et al, 2023. Heart disease and stroke statistics-2023 update: a report from the American heart association. *Circulation*, 147(8): 93–621. https://doi.org/10.1161/CIR.0000000000001123

McEver R P, 2015. Selectins: Initiators of leucocyte adhesion and signaling at the vascular wall. *Cardiovasc. Res.*, 107(3): 331–339. https://doi.org/10.1093/cvr/cvv154

Frodermann V and Nahrendorf M, 2018. Macrophages and cardiovascular health. *Physiol. Rev.*, 98(4): 2523–2569. https://doi.org/10.1152/physrev.00068.2017

Qian H L, Chen S Y, Jia F, et al, 2023. “Spongy skin” as a robust strategy to deliver 4-octyl itaconate for conducting dual-regulation against in-stent restenosis. *Biomaterials*, 296: 122069. https://doi.org/10.1016/j.biomaterials.2023.122069

Inoue T, Croce K, Morooka T, et al, 2011. Vascular inflammation and repair: implications for re-endothelialization, restenosis, and stent thrombosis. *JACC Cardiovasc. Interv.*, 4(10): 1057–1066. https://doi.org/10.1016/j.jcin.2011.05.025

Gaudino M, Antoniades C, Benedetto U, et al, 2017. Mechanisms, consequences, and prevention of coronary graft failure. *Circulation*, 136(18): 1749–1764. https://doi.org/10.1161/CIRCULATIONAHA.117.02759

Wu H S, Yang L, Luo R F, et al, 2024. A drug-free cardiovascular stent functionalized with tailored collagen supports in-situ healing of vascular tissues. *Nat. Commun.*, 15: 735.

https://doi.org/10.1038/s41467-024-44902-2

Zhu J Z, Liu L L, Zhu Z B, et al, 2021. A randomized comparison of a novel iopromide-based paclitaxel-coated balloon shenqi versus sequent please for the treatment of in-stent restenosis. *Coron. Artery Dis.*, 32(6): 526–533. https://doi.org/10.1097/MCA.0000000000000994

Liu S H, Zhi J C, Li S J, et al, 2021. Progress on precise regulation of vascular intimal repair by a surface coating of vascular stent. *Curr. Drug Deliv.*, 18(7): 862–873. https://doi.org/10.2174/1567201818666210212100633

Selestin R I, Kim C, Oh N, et al, 2024. Tailoring photobiomodulation to enhance tissue regeneration. *Biomaterials*, 309: 122623. https://doi.org/10.1016/j.biomaterials.2024.122623

Ma H X, Du Y T, Xie D, et al, 2024. Recent advances in light energy biotherapeutic strategies with photobiomodulation on central nervous system disorders. *Brain Res.*, 1822: 148615. https://doi.org/10.1016/j.brainres.2023.148615

Lee J H, Carpena N T, Kim S, et al, 2021. Photobiomodulation at a wavelength of 633 nm leads to faster functional recovery than 804 nm after facial nerve injury. *J. Biophotonics*, 14(10): 202100159. https://doi.org/10.1002/jbio.202100159

Vasconcelos Catão M H C, Nonaka C F W, Albuquerque R L C, et al, 2015. Effects of red laser, infrared, photodynamic therapy, and green LED on the healing process of third-degree burns: clinical and histological study in rats. *Lasers Med. Sci.*, 30(1): 421–428. https://doi.org/10.1007/s10103-014-1687-0

Lu P, Peng J F, Liu J, et al, 2024. The role of photobiomodulation in accelerating bone repair. Prog. Biophys. *Mol. Biol.*, 188: 55–67. https://doi.org/10.1016/j.pbiomolbio.2024.03.002

Stepanov Y V, Golovynska I, Golovynskyi S, et al, 2022. Red and near infrared light-stimulated angiogenesis mediated via Ca^{2+} influx, VEGF production and NO synthesis in endothelial cells in macrophage or malignant environments. *J. Photochem. Photobiol. B*, 227: 112388. https://doi.org/10.1016/j.jphotobiol.2022.112388

Srinivasan S and Avadhani N G, 2012. Cytochrome *c* oxidase dysfunction in oxidative stress. *Free Radic. Biol. Med.*, 53(6): 1252–1263. https://doi.org/10.1016/j.freeradbiomed.2012.07.021

Passarella S, Casamassima E, Molinari S, et al, 1984, Increase of proton electrochemical potential and ATP synthesis in rat liver mitochondria irradiated in vitro by helium-neon laser. *FEBS Lett.*, 175(1): 95-99. https://doi.org/10.1016/0014-5793(84)80577-3

Greco M, Perlino E, Pastore D, et al, 1991. Helium—neon laser irradiation of rat liver mitochondria gives rise to a new subpopulation of mitochondria: Isolation and first biochemical characterization. *J. Photochem. Photobiol. B*, 10(1):71-78. https://doi.org/10.1016/1011-1344(91)80213-2

Yu W, Naim J O, McGowan M, et al, 1997. Photomodulation of oxidative metabolism and electron chain enzymes in rat liver mitochondria. *Photochem. Photobiol.*, 66(6): 866–871. https://doi.org/10.1111/j.1751-1097.1997.tb03239.x

Karu T I, Pyatibrat L V and Afanasyeva N I, 2005. Cellular effects of low power laser therapy can be mediated by nitric oxide. *Lasers Surg. Med.*, 36(4): 307–314. https://doi.org/10.1002/lsm.20148

Balbi M, Lai R, Stigliani S, et al, 2025. Efficacy and safety of visible and near-infrared photobiomodulation therapy on astenospermic human sperm: wavelength-dependent regulation of nitric oxide levels and mitochondrial energetics. *Biology.*, 14(5):491. https://doi.org/10.3390/biology14050491

Pope N J and Denton M L, 2023. Differential effects of 808-nm light on electron transport chain enzymes in isolated mitochondria: Implications for photobiomodulation initiation. *Mitochondrion*, 68: 15-24. https://doi.org/10.1016/j.mito.2022.11.002.

Farivar S, Malekshahabi T and Shiari R, 2014. Biological effects of low level laser therapy. *J. Lasers Med. Sci.*, 5(2): 58–62. https://www.ncbi.nlm.nih.gov/pmc/articles/PMC4291815/

Chen A C H, Arany P R, Huang Y Y, et al, 2011. Low-level laser therapy activates NF-kB via generation of reactive oxygen species in mouse embryonic fibroblasts. *PLOS ONE*, 6(7): 22453. https://doi.org/10.1371/journal.pone.0022453

De Scheerder I K, Wang K, Kaul U, et al, 2001. Intravascular low-power laser irradiation after coronary stenting: long-term follow-up. *Lasers Surg. Med.*, 28(3): 212–215. https://doi.org/10.1002/lsm.1040

Ma N, Xu E Q, Luo Q, et al, 2023. Rac1: a regulator of cell migration and a potential target for cancer therapy. *Molecules*, 28(7): 2976.
https://doi.org/10.3390/molecules28072976

Zymek P, Bujak M, Chatila K, et al, 2006. The role of platelet-derived growth factor signaling in healing myocardial infarcts. *J. Am. Coll. Cardiol.*, 48(11): 2315–2323.
https://doi.org/10.1016/j.jacc.2006.07.060

Cheng W L, Feng P H, Lee K Y, et al, 2021. The role of EREG/EGFR pathway in tumor progression. *Int. J. Mol. Sci.*, 22(23): 12828.
https://doi.org/10.3390/ijms222312828

Cai X, Liu C, Zhang T N, et al, 2018. Down-regulation of FN1 inhibits colorectal carcinogenesis by suppressing proliferation, migration, and invasion. *J. Cell. Biochem.*, 119(6): 4717–4728.
https://doi.org/10.1002/jcb.26651

Oh K J, Park J, Lee H S, et al, 2018. Effects of light-emitting diodes irradiation on human vascular endothelial cells. *Int. J. Impot. Res.*, 30(6): 312–317.
https://doi.org/10.1038/s41443-018-0051-5

Caldwell R B, Bartoli M, Behzadian M A, et al, 2003. Vascular endothelial growth factor and diabetic retinopathy: pathophysiological mechanisms and treatment perspectives. *Diabetes Metab. Res. Rev.*, 19(6): 442–455.
https://doi.org/10.1002/dmrr.415

Fukumura D, Gohongi T, Kadambi A, et al, 2001. Predominant role of endothelial nitric oxide synthase in vascular endothelial growth factor-induced angiogenesis and vascular permeability. *Proc. Natl. Acad. Sci.*, 98(5): 2604–2609.
https://doi.org/10.1073/pnas.041359198

Yasue H, Nakagawa H, Itoh T, et al, 2008. Coronary artery spasm—clinical features, diagnosis, pathogenesis, and treatment. *J. Cardiol.*, 51(1): 2–17.
https://doi.org/10.1016/j.jjcc.2008.01.001

Wong A, Cheng A, Chan C, et al, 2005. Cardiogenic shock caused by severe coronary artery spasm immediately after coronary stenting. *Tex. Heart Inst. J.*, 32(1): 78–80.
https://pmc.ncbi.nlm.nih.gov/articles/PMC555830/

Lin Z J, Lin X T, Zhao X, et al, 2022. Coronary artery spasm: risk factors, pathophysiological mechanisms and novel diagnostic approaches. *Rev. Cardiovasc. Med.*, 23(5): 175.
https://pmc.ncbi.nlm.nih.gov/articles/PMC11273663/

Rensen S S M, Doevendans P A F M and van Eys G J J M, 2007. Regulation and characteristics of vascular smooth muscle cell phenotypic diversity. *Neth. Heart J.*, 15(3): 100–108.
https://doi.org/10.1007/BF03085963

Yi B C, Shen Y B, Tang H, et al, 2019. Stiffness of aligned fibers regulates the phenotypic expression of vascular smooth muscle cells. *ACS Appl. Mater. Interfaces*, 11(7): 6867–6880.
https://doi.org/10.1021/acsami.9b00293

Kim J I, 2016. High fat diet confers vascular hyper-contractility against angiotensin ii through upregulation of MLCK and CPI-17. *Korean J. Physiol. Pharmacol. Off. J. Korean Physiol. Soc. Korean Soc. Pharmacol.*, 21(1): 99–106.
https://doi.org/10.4196/kjpp.2017.21.1.99

Injeti E R, Sandoval R J, Williams J M, et al, 2008. Maximal stimulation-induced in situ myosin light chain kinase activity is upregulated in fetal compared with adult ovine carotid arteries. *Am. J. Physiol.Heart Circ. Physiol.*, 295(6): 2289–2298.
https://pmc.ncbi.nlm.nih.gov/articles/PMC2614542/

Nohria A, Grunert M E, Rikitake Y, et al, 2006. Rho kinase inhibition improves endothelial function in human subjects with coronary artery disease. *Circ. Res.*, 99(12): 1426–1432.
https://doi.org/10.1161/01.RES.0000251668.39526.c7

Kato M, Blanton R, Wang G R, et al, 2012. Direct binding and regulation of RhoA protein by cyclic GMP-dependent protein kinase Iα*. *J. Biol. Chem.*, 287(49): 41342–4135.
https://doi.org/10.1074/jbc.M112.421040

Nakano T, Osanai T, Tomita H, et al, 2002. Enhanced activity of variant phospholipase c-δ1 protein (R257H) detected in patients with coronary artery spasm. *Circulation*, 105(17): 2024–2029.
https://doi.org/10.1161/01.CIR.0000014613.36469.3F

Shimokawa H and Takeshita A, 2005. Rho-kinase is an important therapeutic target in cardiovascular medicine. *Arterioscler. Thromb. Vasc. Biol.*, 25(9): 1767–1775.
https://doi.org/10.1161/01.ATV.0000176193.83629.c8

Schindl A, Merwald H, Schindl L, et al, 2003. Direct stimulatory effect of low-intensity 670 nm laser irradiation on human endothelial cell proliferation. *British Journal of Dermatology*, 148(2): 334–336.

https://doi.org/10.1046/j.1365-2133.2003.05070.x

Zhang G, Yi L, Wang C X, et al, 2022. Photobiomodulation promotes angiogenesis in wound healing through stimulating the nuclear translocation of VEGFR2 and STAT3. *J. Photochem. Photobiol. B*, 237: 112573. https://doi.org/10.1016/j.jphotobiol.2022.112573

Amaroli A, Ravera S, Baldini F, et al, 2019. Photobiomodulation with 808-nm diode laser light promotes wound healing of human endothelial cells through increased reactive oxygen species production stimulating mitochondrial oxidative phosphorylation. *Lasers Med. Sci.* 34: 495–504. https://doi.org/10.1007/s10103-018-2623-5

Bayat M, Albright R, Hamblin MR, et al, 2022. Impact of blue light therapy on wound healing in preclinical and clinical subjects: a systematic review. *J Lasers Med Sci.*, 13: 69. https://pmc.ncbi.nlm.nih.gov/articles/PMC10082909

Adamskaya N, Dungel P, Mittermayr R, et al, 2011. Light therapy by blue LED improves wound healing in an excision model in rats. *Injury*, 42(9): 917–921. https://doi.org/10.1016/j.injury.2010.03.023

Joensen J, Ovsthus K, Reed R K, et al, 2012. Skin penetration time-profiles for continuous 810 nm and superpulsed 904 nm lasers in a rat model. *Photomed. Laser Surg.*, 30(12): 688-694. https://doi.org/10.1089/pho.2012.3306

Pruitt T, Carter C, Wang X, et al, 2022. Photobiomodulation at different wavelengths boosts mitochondrial redox metabolism and hemoglobin oxygenation: lasers vs. light-emitting diodes in vivo. *Metabolites*., 12(2):103. https://www.mdpi.com/2218-1989/12/2/103

Heiskanen V and Hamblin M R, 2018. Photobiomodulation: lasers vs. light emitting diodes? *Photochem. Photobiol. Sci.,* 17: 1003-1017. https://doi.org/10.1039/c8pp00176f

Salehpour F, Sadigh S, Mahmoudi J, et al, 2023. Biophysical and safety aspects of brain photobiomodulation. in: photobiomodulation for the brain. synthesis Lectures on Biomedical Engineering. Springer, Cham. https://doi.org/10.1007/978-3-031-36231-6_2

Supplementary information

Figs. S1 to S9